INTERNATIONAL ATOMIC ENERGY AGENCY
UNITED NATIONS EDUCATIONAL, SCIENTIFIC AND CULTURAL ORGANIZATION

INTERNATIONAL CENTRE FOR THEORETICAL PHYSICS
34100 TRIESTE (ITALY) - P.O.B. 586 - MIRAMARE - STRADA COSTIERA 11 - TELEPHONES: 224281/2/3/4/5/6
CABLE: CENTRATOM - TELEX 460392-1

SMR/100 - 49

WINTER COLLEGE ON LASERS, ATOMIC AND MOLECULAR PHYSICS

(24 January - 25 March 1983)

Experimental and Theoretical Study of a Femtosecond Laser

B. WILHELMI

Friedrich-Schiller-Universität Jena
Sektion Physik
Max-Wien-Platz, 1
69 Jena
Dem. Rep. Germany

to be published in Kvant. Elektronika

EXPERIMENTAL AND THEORETICAL STUDY OF A FEMTOSECOND LASER [1)]

J.-C. Diels, J. J. Fontaine, I. C. McMichael

North Texas State University
Center for Applied Quantum Electronics
Department of Physics
P. O. Box 5368
Denton, Texas 76203

and

B. Wilhelmi, W. Dietel, and D. Kühlke
Department of Physics
Friedrich Schiller University
Jena, GDR

I. INTRODUCTION

Ultrashort pulse generation with mode-locked dye lasers has proceeded at a surprisingly constant rate, as illustrated in Fig. 1. The mode-locked laser pulse duration has decreased from 500 fsec to 55 fsec in less than a decade. The first laser reported in Fig. 1 has a linear configuration, with a saturable absorber (diethyloxadicarbocyanine iodide or DODCI) jet located near the cavity end opposite to that of a gain medium jet (Rh6G pumped by a CW argon laser). While keeping all the basic components of that laser, small changes in configuration have resulted in significant changes in the mode-locking performance. To improve the cavity loss modulation by saturation, the mode-locked pulse is made to collide with itself in a linear configuration [3], and in all ring lasers [6,8,9]. In a comparison between the linear and the ring configurations, Dietel [10] showed that the "colliding pulse mode-locking" produced pulses that were 4 times shorter. In other schemes, the saturable absorber was mixed with the gain medium in a single jet [4,5,7]. To minimize all bandwidth limitation and pulse broadening by dispersion, all intracavity elements were removed from the cavity [4,5,6,7,8]. However, our recent results demonstrate that an intracavity prism is not necessarily detrimental to the generation of ultrashort pulses in a mode-

1) papers given at National Conference on Coherent and Nonlinear Optics, Jerevan 1982

locked dye laser, but can instead be used for pulse compression [9,11]. While dispersion becomes more important for shorter pulses, so does a phase modulation effect due to saturation of the mode-locking absorber being driven off-resonance. Therefore, in the tunable mode-locked ring dye laser described below, the saturable absorber induces a chirp that causes the pulse to be compressed in the dispersive prism. A description of the laser cavity, its tunability in wavelength and pulse duration follows. Next, we present a theoretical analysis of the mechanism of pulse formation and compression.

II. EXPERIMENTAL DATA

II.1 The Laser Cavity

We have advocated previously [4,5] to avoid any dispersive element as well as any bandwidth limiting element, in the cavity of a short pulse mode-locked dye laser. Intracavity tuning elements were therefore kept out of our cavity, as well as that of the synchronously pumped laser of Sizer and Mourou (pulse duration of 70 fsec [7]) and the ring laser of Fork et al. (pulse duration 65 fsec [8]). The absence of wavelength control being detrimental for some applications, we have studied several cavity configurations incorporating an intracavity tuning prism. In several ring laser configurations that we tested, the tuning element limited the pulse duration to more than 200 fsec. The same limitation was observed in the tunable ring laser reported by Rosen et al. [12]. In the cavity configuration sketched in Fig. 2, the effect of the angular dispersion of the prism is reduced by the curvature of the mirror M3. The less severe bandwidth limitation of this cavity is confirmed by its ability to generate pulses as short as 55 fsec [9]. An accurate calculation of the prism limited bandwidth would require an exact knowledge of the average number of passages through the prism. Since all the cavity mirrors are high reflectors, the Q of the cavity is determined by other losses which are difficult to assess. The prism is mounted on a translation stage, oriented along the bisector of the deviation angle, to provide an adjustment for the thickness of intracavity glass.

The laser is pumped all lines by a 4 W argon ion laser (typical pump powers range from 1 to 3 W). The focussing mirrors have radii of curvature of 3 cm for the saturable absorber and 5 cm for the amplifier jet of Rh6G. A standard coherent radiation jet was used for the gain medium. The jet for the saturable absorber is cut in semicircle, to force a fanout of the liquid escaping from the

nozzle. The thickness of the expending jet decreases with distance from the nozzle. Measurements of jet thickness indicate a minimum of 50 microns at 10 mm downstream from the nozzle.

II.2 Wavelength Tuning

The laser output is monitored with a spectrometer, a fast scanning (30 Hz) autocorrelator, and a slow motion autocorrelator. A surprising observation is that the wavelength of operation of the laser is determined primarily by the concentration of the absorbing dye. For each dye solution, the dispersive prism is adjusted for minimum losses and optical mode-locked operation. The resulting tuning curve is shown in Fig. 3, where the pulse central wavelength is plotted as a function of concentration of the dye 3-3'-diethyloxadicarbocyanine iodide (DODCI) in ethylene glycol. There was no noticable change in the spectral width of the laser output. The solid line is drawn for best fit with the data points. The dashed extension of the solid line indicates a region of instability where the dye laser has a very strong hysteresis. If the lasing operation is interrupted (for instance by blocking shortly the beam inside the cavity), the laser operation resumes only after a long lag time (several seconds).

II.3 Tuning of the Pulse Duration

For each wavelength of operation (determined by the concentration dependence in Fig. 3), the pulse duration can be continuously varied by translating the intracavity prism, thus adjusting the pathlength of glass inside the cavity. The pulse duration, as recorded by the fast scanning autocorrelator, is plotted versus intracavity glass thickness for three different wavelengths of operation, in Fig. 4. At all wavelengths, we observe a minimum in the dependence of pulse duration versus glass thickness. The position of the minimum - i.e., the pathlength at minimum pulse duration - also shows a minimum. The shortest pulse duration recorded at each wavelength, varies across the tuning range. With the

quartz prism used in the measurements of Fig. 4, the wavelength dependence of the pulse duration at the minima, shows a minimum at 617 nm. The minimum duration pulses are less than 100 fsec in the range from 605 nm to 620 nm. The value of the minimum could not be determined beyond 620 nm because the maximum pathlength in the quartz prism used was 10 mm, not sufficient to reach the minimum beyond 620 nm. The data shown in Fig. 4 were recorded with the fast scanning autocorrelator, and have therefore an accuracy not better than 20%. A more accurate slow scan of the pulse autocorrelation at minimum pulse duration is shown in Fig. 5.

We do not observe any significant change in pulse spectrum for all the data of Fig. 4, and the spectral width indicates that the shortest pulses are bandwidth limited. A constant spectral width is consistent with the interpretation given below that the pulses are downchirped for shorter glass pathlength than optimum; upchirped for longer pathlength. However, we believe that linear spectral information has only limited value because of the very small duty cycle of the laser. Indeed, any signal between the femtosecond pulses, of more than 10 pJ energy, will contribute more to the spectrum than the femtosecond pulses themselves. Work is in progress to obtain spectra with second harmonic detection. We performed interferometric second order autocorrelations [5] to verify that the longer pulses are indeed phase modulated.

In order to verify that the mechanism of ultrashort pulse formation involved intracavity pulse compression in glass, we measured the pulse duration after transmission through various thicknesses of heavy flint glass (SF5). With a small intracavity pathlength (1.8 mm), the dependence of pulse duration versus thickness of SF5 glass (extracavity) shows a minimum for a thickness of 200 mm. If the intracavity pathlength exceeds that corresponding to a minimum pulse duration (8 mm quartz for the second curve of Fig. 6), only normal pulse

broadening through dispersion is observed in the extracavity glass. The difference in glass type (normal dispersion) probably explains that the second curve (circles) is not exactly a mere displacement of the first one (triangles). Measurements such as shown in Figs. 4 and 6 indicate that 1 mm intracavity quartz corresponds to 23 of extracavity flint glass. Since the mechanism of compression is related to the normal dispersion of glass as discussed below, 32 mm of SF5 glass is equivalent to 95 mm of quartz. The ratio of extracavity to intracavity length of glass (1 to 95) corresponds to a cavity lifetime of 950 nsec.

III.1 Introduction

The theory detailed below explains most of the characteristics of the passively mode-locked dye laser. Included in the model are the saturation of the gain and absorbing media responsible for mode-locking. The lineshape of both the amplifying and absorbing media are approximated by Lorentzians. In the case of the ring laser where two counterpropagating pulses "collide" in the absorber jet, the population grating induced in the medium causes a coupling between the two pulses. It is shown that this coupling results in pulse compression, as long as the pulse duration is long compared with the medium thickness. The compression mechanism disappears, as demonstrated by computer simulations, for pulses short compared with the medium thickness. The bandwidth limiting properties of the amplifier and absorber as well as that of other optical elements (prism, mirrors), are "lumped" in an effective frequency filter. In order to understand the influence of a glass pathlength on pulse compression, we note that the saturable absorber is excited below resonance. Therefore, saturation of the dispersion results in a susceptibility decreasing with time, which causes the pulse to be "downchirped". When a pulse with such a frequency modulation propagates through a medium with normal dispersion, the pulse tail propagates faster than the pulse front (at higher frequency, thus subject to a larger susceptibility), resulting in pulse compression and chirp compensation.

III.2 Basic Equations:

As in our previous work [13,14,15,16], a semiclassical approach [17] is used to model the interaction between radiation and the media. We shall first consider the absorber length to be small compared to the pulse length. A stationary regime is postulated, where two counterpropagating pulses circulate in a ring resonator (Fig. 7) and meet exactly in the absorber. This situation

corresponds to the lowest loss regime of the ring laser. The line shapes of the absorbing and amplifying media are fitted to Lorentzians centered respectively at ω_a and ω_g. For the counterpropagating pulses, we assume plane waves centered at a frequency ω_L, with slowly varying complex amplitudes A_1 and A_2. The absorber is represented by a two-level system (Fig. 8) with a negligible population in the excited vibrational level of the S_1 state. The phase relaxation times are taken to be short with respect to the pulse duration, an assumption that is justified for broadband dyes up to the subpicosecond range. In the following equations quantities refering to the amplifier (absorber) are labelled by the index g(a), and the real (imaginary) parts of complex quantities by the index r(i). Using for the electric field for the counterpropagating waves

$$E(z,t) = \frac{1}{2}\left[A_1(z,t)\, e^{-ikz} + A_2(z,t)\, e^{ikz}\right] \quad e^{-i\omega_L t} + c.c. \tag{1}$$

the density matrix equation yields the following rate equation for the population of the absorber ground level:

$$\frac{\partial n_1^a}{\partial t} = -\beta_a\, n_1^a\, \mathcal{L}_a^r \left[|A_1|^2 + |A_2|^2 + A_1^* A_2\, e^{2ikz} + A_1 A_2^*\, e^{-2ikz}\right] \tag{2}$$

$$+ \frac{n^a - n_1^a}{T_{21}^a}$$

where $n^a = n_1^a + n_2^a$ is the particle number density, $\beta_a = T_{13}^a |\mu_{13}^a|^2 / 2\hbar^2$, $\mathcal{L}_a^r$ is the real part of $\mathcal{L}_a = [1 - 2i(\omega_a - \omega_L)/\Delta\omega_a]^{-1}$, which describes the line profile of width $\Delta\omega_a = 2/T_2$ of the absorber transition, μ_{13}^a and T_{13}^a are the dipole matrix element and the phase relaxation time, respectively. Equations 2 provide the

first coefficient q, p of the spatial Fourier expansion $n_1^a = q + pe^{-2ikz} + p^* e^{2ikz}$ for the relations

$$\frac{\partial q}{\partial t} = -\beta_a \mathcal{L}_a^r \{q(|A_1|^2 + |A_2|^2) + p A_1^* A_2 + p A_1^* A_2|^* + \frac{n^a - q}{T_{21}^a} \quad (3)$$

$$\frac{\partial p}{\partial t} = -\beta_a \mathcal{L}_a^r [p(A_1^2 + A_2^2) + q A_1^* A_2] - \frac{p}{T_{21}^a} \quad (4)$$

Using Maxwell's equations with the electric field (1) we find in the rotating wave approximation, equations for the slowly time-varying complex amplitudes:

$$(\frac{-\partial}{\partial z} + \frac{1}{v} \frac{\partial}{\partial t}) A_1 = -\frac{1}{2} \sigma^a \mathcal{L}_a (q A_1 + p A_2) \quad (5)$$

$$(\frac{\partial}{\partial z} + \frac{1}{v} \frac{\partial}{\partial t}) A_2 = -\frac{1}{2} \sigma^a \mathcal{L}_a (q A_2 + p^* A_1) \quad (6)$$

$\sigma^a = 2\hbar\omega_L \sqrt{\mu_o/\varepsilon_o}\, \beta_a$ is the cross-section at the center of the absorber line and v is the group velocity of the sample under investigation (without taking into account the influence of the quasi resonant transitions or of the bandwidth limiting element). Equation (3) - (6) are solved by successive approximation using the same procedures as in Ref. 18. Assuming that the energy relaxation time of the absorber is long compared with the pulse duration τ, and short compared with the cavity round trip time U, the relaxation term in (3) and (4) can be neglected. The small signal absorption is supposed to be small compared to unity. Keeping terms up to second order in the pulse energy normalized to the saturation energy, we find an approximate solution of (2) - (6) of the form

$$A_2(\eta,2) = 1 - \frac{1}{2}\alpha_o [1 - m(E_1+E_2) + m^2 [\frac{1}{2}(E_1^2+E_2^2) + E_1E_2 + E_{12}E_{21}]] A_2(\eta,1)$$
$$+ \frac{1}{2}\alpha_o m E_{21} (1 - m(E_1 + E_2)) A_1(\eta,2) \quad (7)$$

$$E_{k\ell} = \frac{\sigma^g \mathcal{L}_g^r}{2\hbar\omega_L} \sqrt{\frac{\varepsilon_o}{\mu_o}} \int_{-\infty}^{+\eta} d\eta' A_k(\eta') A_\ell^*(\eta')$$

$E_{\ell\ell} = E_\ell$

$(\ell = 1,2)$

$m = u \frac{\sigma^a \mathcal{L}_a^r}{\sigma_g \mathcal{L}_g^r}$, $\eta = t \pm \frac{z}{v}$ in both media.

$\alpha_o = \alpha_a \mathcal{L}_a$ defines the complex small signal attenuation coefficient, z is the absorber thickness, and α_a is the small signal absorption at the center of the absorption band. The equation for pulse 1 follows from (7) by exchanging the indices 1 and 2.

The interaction of the laser pulse with the amplifier is also described by rate equations. Unlike the absorber the gain medium interacts only with one unidirectional pulse at any time. The amplifier is assumed to be not fully relaxed before the next pulse arrives. For small pulse energies and weak small signal gain the pulse amplification during one cavity round trip is given by

$$A_2(\eta,1) = [1 + \frac{1}{2}\alpha_2(1 - E_2)] A_2(\eta,0) \quad (8)$$

with a corresponding equation for A_1. The complex gain coefficients at the leading edge of the pulse 1 and 2 are

$$\alpha_1 = \mathcal{L}_g \alpha_o \left\{1 - \frac{\varepsilon_1 + \varepsilon_2 \exp[(U - 2\delta)/T_{21}^g]}{\exp(U/T_{21}^g) - 1}\right\} \quad (9)$$

$$\alpha_2 = \mathcal{L}_g \alpha_o \left\{1 - \frac{\varepsilon_2 + \varepsilon_1 \exp(2\delta/T_{21}^g)}{\exp(U/T_{21}^g) - 1}\right\} \quad (10)$$

respectively, where δ is the transit time between the absorber and amplifier, $\epsilon_2 = E_1(\eta \to \infty)$ is the pulse energy normalized to the saturation energy of the amplifier per unit area $\hbar\omega_L/\sigma_g^{\ell r}$, T_{21}^g is the energy relaxation time of the amplifier and α_o represents the small signal gain at the center of the gain line. The influence of the effective filter is characterized by its transfer function $H(\omega - \omega_d) = [1 + 2i(\omega - \omega_d)/\Delta\omega]^{-1}$ and is supposed to contain all the bandwidth-limiting properties of the cavity. If the pulse spectrum is narrow compared with the spectral width $\Delta\omega$ of the filter, and also centered at ω_d (the center frequency ω_d of the filter transmittance profile), the change of the pulse shape after each passage through this element is given by:

$$A_2(\eta,3) = \left[1 - \frac{2}{\Delta\omega}\,\frac{d}{d\eta} + \frac{4}{\Delta\omega^2}\,\frac{d^2}{d\eta^2}\right] A_2(\eta,2) \tag{11}$$

The effect of linear losses γ due to the outcoupling mirror on the pulse shape is given by

$$A_2(\eta,4) = \left(1 - \frac{1}{2}\gamma\right) A_2(\eta,3) \tag{12}$$

Steady-state condition requires that the pulse shapes reproduce themselves after each cavity round trip, with a possible shift h in local time. For $h \ll \tau$ this gives

$$A_2(\eta,4) = A_2(\eta + h,0)\quad\left[1 + h\frac{d}{d\eta} + \frac{1}{2}h^2\frac{d^2}{d\eta^2}\right] A_2(\eta,0) \tag{13}$$

Substitution of Eqs. (7) - (12) into Eq. (13) leads to the following integrodifferential equation for the steady-state pulse shapes $A(\eta,0)$:

$$\left[g_2 - \left(h + \frac{2}{\Delta\omega}\right)\frac{d}{d\eta} + \left(\left(\frac{2}{\Delta\omega}\right)^2 - \frac{h^2}{2}\right)\frac{d^2}{d\eta^2}\right] A_2(\eta,0)$$

$$+ f_{21} A_2(\eta,0) = 0 \tag{14}$$

where

$$g_2 = \frac{1}{2}\left[\alpha_2 - \mathcal{H}_o - \gamma - (\alpha_2 - \mathcal{H}_o m)\,E_2 + \mathcal{H}_o m\,E_1\right.$$

$$\left. - \mathcal{H}_o m^2\left(\frac{1}{2}(E_1^2 + E_2^2) + E_1E_2 + E_{12}E_{21}\right)\right] \tag{15}$$

and

$$f_{21} = \frac{1}{2}\,\mathcal{H}_o m\,E_{21}(1 - m(E_1 + E_2)) \tag{16}$$

We will generally consider the ideal situation where the absorber-amplifier distance is exactly one quarter of the perimeter ($\delta = U/4$). In that particular case, the amplification for both directions being equal, i.e., $\alpha_1 = \alpha_2 = \alpha$, both counter propagating pulses are identical in amplitude and shape ($A_1 = A_2 = A$; $E_1 = E_2 = E$). We can obtain a coupled system of nonlinear integro-differential equations for the time dependent amplitude $|A(\eta)|$ and phase $\phi(\eta)$ of the pulse

$$A(\eta) = |A(\eta)|e^{i\phi(\eta)}$$

by separating the real and imaginary parts of Eq. (14).

III.3 Physical Interpretation of the Pulse Shortening in the CPM-Regime

The saturation behavior of the absorber essentially determines the pulse shaping in passive mode-locking. Therefore we want to discuss and compare

various mechanisms affecting the absorber saturation for the case of resonance ($\omega_1 = \omega_a = \omega_g$). The simplest model is that of one pulse circulating in the ring resonator. It is described by Eqs. 7 - 10 with $A_1 = 0$, $A_2 = A$, and $\alpha = \alpha_2$, $\mathcal{H}_o$ being real quantities. Here the relations describing the influence of the amplifier (Eq. 8)

$$A(n,1) = (1 + \tfrac{1}{2}\alpha(1 - E))\, A(n,0) \tag{17}$$

and of the absorber (Eq. 7)

$$A(n,2) = [1 - \tfrac{1}{2}\mathcal{H}_o\,(1 - mE + \tfrac{1}{2}(mE)^2)]\, A(n,1) \tag{18}$$

have the same structure, i.e., the saturation behavior of both the media differs only due to their different saturation energies (described by m [illegible]). The case of counter-propagating pulses superimposed in the absorber is obtained from Eqs. 7 - 10 with $\alpha_{1,2} = \alpha$, and $\mathcal{H}_o$ real. To determine the influence the saturation behavior of the absorber we first drop the terms describing the coherent interaction of the counter running pulses in the absorber ($E_{12} = 0$). Then Eq. 7 reads

$$A(n,2) = 1 - \tfrac{1}{2}\mathcal{H}_o\,[1 - m2E + \tfrac{1}{2}(m2E)^2]\;\; A(n,1) \tag{19}$$

Due to the special pulse sequence in the absorber and the amplifier the absorber is saturated by almost twice the energy that affects the amplifier. This is a straightforward consequence of our original assumption that the absorber thickness be small compared with the pulse length. Departure from that condition will be briefly discussed in section III.4. Terms containing E_{12} in Eq. 7 describe the effect of the transient standing wave field formed by the counter-

running pulses. This standing wave field leads to a spatially periodic saturation modulation of the population of the absorber that acts as an amplitude grating. The last term on the right hand side of Eq. 7 or the last term on the left hand side of Eq. 14 has the structure of a reflection term and it describes the part of pulse 1 reflected by this grating into the direction of pulse 2. The constructive interference between the reflected and original waves modify the saturation behavior of the absorber. Additionally Eq. 7 written with $A_1 = A_2 = A$ as

$$A(n,2) = [1 - \tfrac{1}{2}\mathcal{H}_o\,(1 - 3mE + 5\,(mE)^2)]\, A(n,1) \tag{20}$$

makes this obvious. To meet this situation in experiments the absorber length is required to be of the order of or less than the pulse length so that the coherent pulse interaction becomes essential (CPM with short absorbers). Taking Eqs. 18, 19, or 20 instead of Eq. 7 to obtain the relation for the steady state pulse amplitudes and solving it approximately by the secant-hyperbolic ansatz [19]

$$A(n,0) = \sqrt{\sqrt{\frac{h_o}{\varepsilon_o}}\;\frac{\hbar\omega_L\,\varepsilon}{\sigma^a\,\alpha_a\,\rho\,r_\tau}}\;\;\frac{1}{\cosh\,(n/\tau)} \tag{21}$$

we can determine the pulse energy ε and the pulse duration τ. Figure 9 shows the dependence of the pulse duration on the small signal gain for the three cases. It is obvious, that the influence of the transient grating and the resulting coherent interaction of the counter-propagating pulses leads to a further pulse shortening and to an increase of the stability range. The numerical calculations have shown that the differences in the stability ranges and pulse durations between the three cases decrease with increasing ratio of the

saturation energies m. But for all m the pulses become shortest in the CPM with short absorber. For $\omega_L = \omega_a = \omega_g$ the CPM regime with counter-propagating pulses of equal as well as of different amplitudes have been treated in detail [13]. Therefore we will restrict ourselves to the case of pulses with equal amplitudes and concentrate on the influence of the time dependent phase. The complex Eqs. (14) with (17) are satisfied by the ansatz (see [14])

$$A(\eta) = \sqrt{\frac{\mu_o}{\epsilon_o}} \frac{\pi \omega_L \varepsilon}{\sigma^a \mathcal{L}_a r_\tau} \frac{1}{\cosh(\eta/\tau)} \tag{22}$$

and

$$\frac{d\phi(\eta)}{d\eta} = \frac{a}{\tau} + \frac{b}{\tau} \tanh(\eta/\tau) \tag{23}$$

In Eq. (23) a/τ represents a deviation from the frequency ω_L determined by the resonator without taking into account the quasi resonant transitions. This deviation is caused by the dispersion of the absorber and amplifier transition, i.e., $\omega_L - a/\tau$ is now the center frequency of the pulse at $\eta = 0$. The term $(b/\tau) \tanh(\eta/\tau)$ describes the instantaneous frequency shift from the center frequency of the pulse at the local time η. Consequently $\delta = 2b/\tau$ gives the total frequency shift from the leading edge to the trailing edge of the pulse; $b > 0$ corresponds to "down chirp" and $b < 0$ to "up chirp". Substituting (22), (23) into (14) with (17) one obtaines a system of six algebraic equations for ε, τ, h, a, b, ω_L. Especially for the chirp parameter b an expression of the form

$$b = \frac{3\mathcal{H}_r}{2\mathcal{H}_i} \pm \sqrt{\left(\frac{3\mathcal{H}_r}{2\mathcal{H}_i}\right)^2 + 2} \tag{24}$$

is found, where the sign + applies for $\mathcal{H}_i < 0$ and - for $\mathcal{H}_i > 0$. Figures 10 shows that there are two frequency regions for the set of parameters choosen where a stable signal pulse regime occurs. The two solutions differ by the energy of the generated pulses (Fig. 11). For the solution with the greater energy the pulse duration, the deviation from ω_L and the chirp parameter are depicted in Figs. 12 and 13, respectively. To compare these results with the experimental data of the passively mode-locked cw dye laser with Rh 6G as amplifier and DODCI as saturable absorber the following values of the parameters are used: $\omega_g = 3.2410^{15}\ s^{-1}$, $\Delta\omega_g = 0.18\ 10^{15}\ s^{-1}$, $\omega_a = 3.22\ 10^{15}\ s^{-1}$, $\Delta\omega_a = 0.115\ 10^{-15}\ s^{-1}$, $\Delta\omega = 0.31\ 10^{15}\ s^{-1}$. These values have been estimated by fitting in the frequency range under consideration Lorentzian profiles to the fluorescence profile of Rh 6G, the absorption profile of DODCI. The filter profile results from the difference of the fluorescence and absorption profile where both the profiles are appropriately weighted.

From Fig. 10 it is obvious that a stable single pulse regime should appear in the wavelength ranges of 596 - 602 nm and 612 - 624 nm. This roughly corresponds to the experimental range of about 600 - 625 nm, where passive mode-locking occurs. A qualitative description of the dependence of the pulse wavelength on the DODCI concentration reported above in section II.2 (Fig. 3) is shown in Fig. 10b. From Fig. 12 the half width $\tau_{FWHM} = 1.76\,\tau$ of the pulses is deduced to the within the ranges of 58 - 89 fs for $m_o = 5$ and 50 - 82 fs for $m_o = 6$ (it should be noted that $m_o = 5$ and 6 respectively corresponds to a ratio $m = m_o \mathcal{L}_a r / \mathcal{L}_g r$ (of about 3.0 - 3.3 and 3.7 - 4.3) of the saturation energies of both media in the wavelength range of mode-locking shown in Fig. 10. This ratio corresponds to our experimental parameters. These pulse durations agree well with the ones experimentally obtained by various authors (90 fs [6], 85 fs [11], 65 fs [8], 53 fs [9]).

III.4 Influence of a Finite Jet Thickness

Even in the case of nonresonant (instantaneous response time) nonlinear susceptibilities, the dynamics of the transient four wave mixing becomes very complex in media of finite thickness [20]. The transient grating formation in a thick saturable absorber is even more complex, and can only be studied numerically. We have made numerical calculations of the mutual interaction of two counterpropagating pulses in such a medium, using a similar predictor corrector method as used in [20]. Two effects arise from the finite jet thickenss:

1. A significant pulse reshaping takes place. The pulse leading edge steepens, while the tail becomes longer.
2. With increasing absorber thickness, the pulse ceases to be compressed.

The computation of counterpropagating interaction in the absorber was included in a program simulating the operation of the whole dye laser [16] assuming resonant interaction. The limiting influences of the finite jet thickness on the minimum pulse duration was demonstrated. Further work is in progress to study the influence of the saturation parameter on the counterpropagating interaction on- and off-resonance.

III.5 Pulse Chirp and Chirp-Compensation:

Equation 24 shows that the frequency sweep during the pulse duration is positive for $\omega_L > \omega_a$ ($b < 0$, up-chirp) and negative for $\omega_L < \omega_a$ ($b > 0$, down-chirp). In mode-locked cw dye lasers with rhodamine 6G and DODCI the lasing wavelength is red-shifted with respect to the absorber transition, i.e., the pulses generated are expected to be down-chirped which is in agreement with experimental results [9,11]. From Fig. 13 the parameter b/τ is estimated to be within the range of $1.7 \times 10^{13} - 2.2 \times 10^{13}\ s^{-1}$, which corresponds to a wavelength shift during the half width of the pulses of 4.9 - 6.2 nm. These values are greater than the wavelength shift of about 1 nm experimentally determined by

Dietel et al. [11]. However, it should be noted, that the wavelength sweep is partially compensated by the glass path of the intracavity prism in the experimental set up of [9].

An estimate of the real wavelength sweep is possible by use of the experimental data presented in section II.3. For this the relation between the autocorrelation width τ_{in} of an incident pulse with frequency-sweep $\delta\omega$ during its duration (FWHM) and width τ_{min} of the pulse after the chirp has been compensated by a pass length L^{min} in glass is used [8]. It is

$$\tau_{min} = \tau_{in} \left[1 + \frac{1}{2} \left(\delta\omega\tau_{in}/2\ln 2\right)^2\right]^{-\frac{1}{2}} \tag{25}$$

To compensate a frequency-sweep $\delta\omega$ of a pulse with a width τ_{in} a glass length

$$L^{min} = \frac{\pi c^2 \tau_{in}}{\sqrt{2}\,\lambda^3\, n''\, \left[1 + 2\left(\frac{2\ln 2}{\delta\omega\tau_{in}}\right)^2\right]} \tag{26}$$

is required. These relations are exactly valid for Gaussian-pulses with linear chirp. They are supposed, however, to approximately describe the dye laser pulses under consideration, too. Taking the values $\tau_{FWHM}^{(in)} = 73$ fs, $\tau_{FWHM}^{(in)} = 300$ fs for $\lambda_L = 615$ nm (Fig. 1 of Ref. 6) we obtain with $\tau = 1.55\ \tau_{FWHM}$ the frequency sweep $\delta\omega = 1.74 \times 10^{13}\ s^{-1}$ which corresponds to a wavelength sweep of about 3.5 nm. This value is close to the one estimated above, by the theoretical calculations. The goal is to compensate the down chirp in order to obtain pulses of minimal duration. This can be done by pulse compression in an extracavity glass as well as by chirp compensation in an intracavity glass path. This means a down chirp must be compensated that arises in the first case from a multiple pass and in the second case from a single pass through the nonlinear media. The correspondence of extracavity to intracavity length of glass (95 to

1) reflects this. From Eq. 26 an extracavity glass length $L^{min} \simeq 160$ mm of fused silica ($n'' = 1.55 \times 10^{11}$ m^{-2}) is estimated to compensate the down-chirp of 5 nm of a pulse with $\tau_{FWHM} \simeq 400$ fs. By means of Eq. 7 we can determine the wavelength sweep of a pulse arising from a single pass through the saturable absorber. The change of the pulse phase due to passing the absorber is obtained to be

$$\phi(\eta,2) - \phi(\eta,1) = -\frac{1}{2}\mathcal{H}_o^i \left[1 - 3mE(\eta,1) + 5(mE(\eta,1))^2\right] \qquad (27)$$

If the incoming pulse is sech^2-shaped with a time independent phase ($\phi(\eta,1) = \text{const}$) we obtain from Eq. (27)

$$\frac{d\phi(\eta,2)}{d\eta} = \frac{\mathcal{H}_o^i\, m\varepsilon}{4T\cosh^2(\eta/\tau)}\,(3 - 5\, m\varepsilon(1 + \tanh(\eta/\tau)) \qquad (28)$$

which results in a frequency sweep during the pulse duration ($\tau_{FWHM} = 1.76\,\tau$) of $+1.56\,\mathcal{H}_o^i\,(m\varepsilon)^2/\tau_{FWHM}$. For $m = 3$, $\varepsilon = 0.1$, $\mathcal{H}_o = 0.4, 2(\omega_L - \omega_a)/\Delta\omega_a \simeq -1.35$ (i.e., $\lambda_L \simeq 615$ nm) and $\tau_{FWHM} = 100$ fs this gives $\delta\omega \simeq -3 \times 10^{11}$ s^{-1} which corresponds to a wavelength sweep of $\delta\lambda_L \simeq -0.05$ nm. To compensate this downchirp a glass length of fused quartz ($n'' = 1.35 \times 10^{11}$ m^{-2}) of $L_{min} \simeq 2$ mm is required (cf Equation 26). The calculated ratio $(L_{min})_{extracavy}$ to $(L_{min})_{intracavy}$ of 80 roughly agrees with the ratio 95 measured in section II.3.

IV. CONCLUSIONS

A ring laser has been demonstrated that is tunable in pulse duration from 1 ps down to 55 fs, in wavelength from 615 to 624 nm, and in down chirp from 0 to 5 nm. The pulse duration is adjusted by varying the pathlength in an intracavity prism. The chirp can also be adjusted this way, or alternately, by adjusting the extracavity path length in glass. Such control is important if bandwidth limited pulses are desired from extracavity optical systems incorporating dispersive elements. The intracavity prism provides some wavelength control, but the wavelength at which one obtains optimum performance in terms of both pulse duration and stability is mostly determined by the saturable absorber concentration.

A theoretical model of passively modelocking that includes grating effects in CPM is presented. The only input to the theory are the absorber and amplifier characteristics, and a filter. The theory predicts the stability range and pulse duration as a function of the small signal gain for the case of unidirectional operation and for CPM with both long and short absorbers. In agreement with experiment, it is shown that the shortest and most stable pulses are generated in CPM. The theory also predicts that the pulses will have a chirp due to the dispersion of the amplifier and absorber transitions. This model was applied to the specific case of R6G as the amplifier and DODCI as the absorber. The theory predicts stable modelocking in the wavelength region 596-602 nm and 612-624 nm. This is roughly in agreement with experiment. The theory also predicts the observed down chirp. Calculations of the expected pulse duration after passage through glass, both intra and extra cavity, are in good agreement with our experiments. The theory, however, does not explain the particular wavelength dependence of the down chirp, that is observed experi-

mentally. It is not clear why the down chirp should have a minimum between 615 and 620 nm.

We expect that further extension of these principles of down chirping and compression through the selection of appropriate amplifying media, absorbing media, and intracavity dispersive elements, will lead to a better control of the pulse duration, phase modulation and average frequency.

REFERENCES

1. C. V. Shank and E. P. Ippen, Appl. Phys. Lett. 24, 373 (1974).
2. E. P. Ippen and C. V. Shank, Appl. Phys. Lett. 27, 488 (1975).
3. I. S. Ruddock and D. J. Bradley, Appl. Phys. Lett. 29, 296 (1976).
4. J.-C. Diels, E. W. Van Stryland, and G. Benedict, Optics Comm. 25, 93 (1975).
5. J.-C. Diels, J. Menders, and H. Sallaba, Proceedings of the 2nd Int. Conf. on Picosecond Phenomena, Springer-Verlag, 41 (1980); J.-C. Diels, Proceedings of the Conf. on Ultrashort Phenomena in Spectroscopy, Reinhardsburn, published by G. Wilhelmi, Jena University, 527 (1981).
6. R. L. Fork, B. I. Green, and C. V. Shank, Appl. Phys. Lett. 38, 671 (1981).
7. G. A. Mourou and T. Sizer II, Optics Comm. 41 47 (1982).
8. C. V. Shank, XIIth Int. Quantum Electronics Conference, paper K2.1, June 22, Munich (1982).
9. W. Dietel, J. J. Fontaine, and J.-C. Diels, Optics Letters, 8, 4 (1983).
10. W. Dietel, Optics. Comm. 43, 69 (1982).
11. W. Dietel, E. Dopel. D. Kuhlke, and B. Wilhelmi, Optics Comm. 43, 433 (1982).
12. D. Rosen, A. G. Doukas, Y. Budansky, A. Katz, and R. R. Alfano, IEEE J. of Quant. Electronics, Vol. QE-17, 2264 (1981).
13. D. Kuhlke, W. Rudolph. B. Wilhelmi, submitted to IEEE J. of Quant. Electro. (Special Issue on Picosecond Phenomena).
14. D. Kuhlke, W. Rudolph, to be published in Opt. Quant. Electr.
15. W. Dietel, D. Kuhlke, W. Rudolph. B. Wilhelmi, kvant. elektronika, in press.
16. J.-C. Diels, I. C. McMichael, J. J. Fontaine, and C. Y. Wang, Proceedings of the Third Int. Conf. on Picosecond Phenomena, 116 (Springer-Verlag,

Berlin, 1982).

17. J. A. Fleck, J. Appl. Phys. 39 (1968) 3318.

18. J. Hermann, F. Weidner, B. Wilhelmi, Appl. Phys. B 26 (1981) 197.

19. H. A. Haus, IEEE J. Quant. Electron. QE-11 736 (1975).

20. J.-C. Diels, W. C. Wang, and H. Winful, Appl. Phys. B 26, 105 (1981).

FIGURE CAPTIONS

Figure 1 Improvements in subpicosecond pulse generation in the last decade; + = direct output from the laser; (+) = pulse duration achieved after pulse compression (Ref. 1 - 9).

Figure 2 Cavity configuration. The argon pump mirror has a radius of curvature of 3 cm. The focussing mirrors around the amplifying and absorbing jets are respectively M1 and M2 = 5 cm, and M4 and M5 = 3 cm. The cavity mirror M3 has a radius of curvature of 1 m. The perimeter of the resonator is 3.6 m.

Figure 3 Wavelength of operation of the mode-locked laser versus concentration of DODCI is ethylene glycol. The dashed line indicate a region of hystersis and and instability.

Figure 4 Pulse duration versus intracavity pathlength in BK7 glass for three operating wavelengths of the laser (saturable absorber: DODCI).

Figure 5 Second order autocorrelation of the pulse train, with a peak to background ratio of 3 to 1. The autocorrelation width of 82 fsec corresponds to a sech^2 pulse duration of less than 55 psec.

Figure 6 Pulse duration versus extracavity pathlength in SF_5 glass, for two different intracavity pathlengths of quartz. The wavelength of operation is 620 nm.

Figure 7 Sketch of the ring laser with amplifier A_1 saturable absorber B_1 bandwidth limiting element C and an out coupling mirror D. $A_{1,2}$ are the amplitudes of the counter-running pulses.

Figure 8 Energy levels of the saturable absorber.

Figure 9 Pulse duration τ normalized to the inverse band width $\Delta\omega^{-1}$ of the effective filter versus small signal gain α_o for the cases of a

unidirectional pulse regime (curve a, $\mathcal{A}_o = 0.135$), of a CPM-regime with long absorber (curve b, $\mathcal{A}_o = 0.12$) and of a CPM-regime with short absorber. The dashed lines denote the boundaries of the stable single pulse regime. The other parameters used are $m = 2$, $\gamma = 0.01$ and $\Delta = 2.03$ (i.e., the ratio U/T_{11}^a has been chosen so that for the three cases the amplifier is relaxed in the same way before entering of the pulse).

Figure 10a Detuning from the center frequency of the absorber versus small signal gain α_o where stable single pulse regimes occur ($m_o = 6$, $\mathcal{A}_o = 0.4$, $\gamma = 0.015$, $U/T_{21}^g = 0.8$, $2(\omega_a - \omega_g)/\Delta\omega_a = 0.174$, $\Delta\omega_a/\Delta\omega_g = 1.56$). The lasing wavelength λ_L on the right hand ordinate has been determined for $\Delta\omega_a = 0.22 \times 10^{15}\ s^{-1}$ and $\omega_a = 3.22 \times 10^{15}\ s^{-1}$.

Figure 10b Detuning from the absolute frequency versus small signal absorption $\mathcal{A}_o$ for $\alpha_o = 0.4$, $m_o = 5$. The other parameters are the same as for Fig. 4a. For a comparison the measured DODCI concentration dependence of the wavelength of a passively mode-locked cw dye laser is depicted (circles). However it should be noted that the experimental conditions for the data are unknown. (The dependence assumed between the DODCI concentration and $\mathcal{A}_o$ corresponds to an absorber thickness of about 25 μm).

Figure 11 Pulse energy ε versus small signal gain for the two solutions depicted in Fig. 10a. It should be noted that the range of the small signal gain α_o at the line center of 0.335 - 0.445 corresponds to a range of the small signal gain in the region of the lasing wavelength of $\alpha_o^r = \alpha_o \mathcal{L}_a^r$ of 0.13 - 0.25 and the small signal absorption $\mathcal{A}_o = 0.4$ to a range of $\mathcal{A}_o^r = \mathcal{A}_o \mathcal{L}_b^r$ of 0.1 - 0.16.

Figure 12 Pulse duration τ normalized to the inverse bandwidth $\Delta\omega^{-1}$ versus small signal gain α_o for $m_o = 5$ (curve a) and $m_o = 6$ (curve b). The other parameters are the same as for Fig. 10a.

Figure 13 Chirp parameter b/τ (curve a) and frequency shift a/τ (curve b) normalized to $\Delta\omega^{-1}$ versus small signal gain α_o.

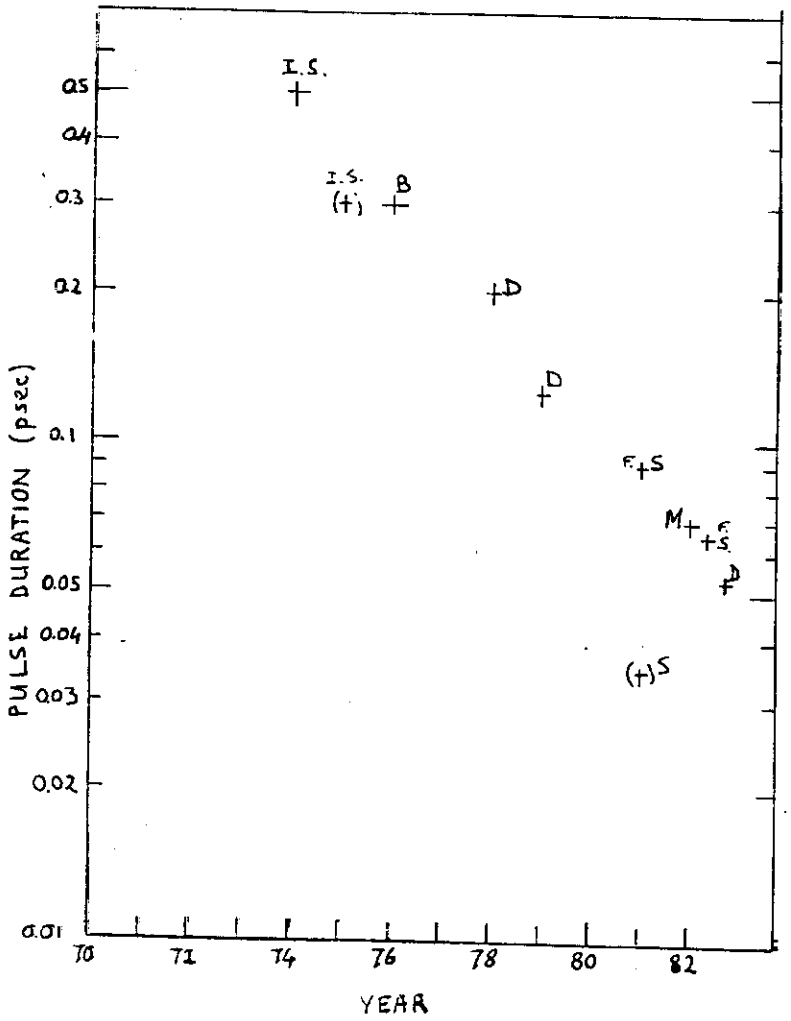
PULSE DURATION (psec)
0.5
0.4
0.3
0.2
0.1
0.05
0.04
0.03
0.02
0.01
70
72
74
76
78
80
82
YEAR
I.S.
I.S.
(+)
B
D
D
F
S
M
S
F
S
(+)S

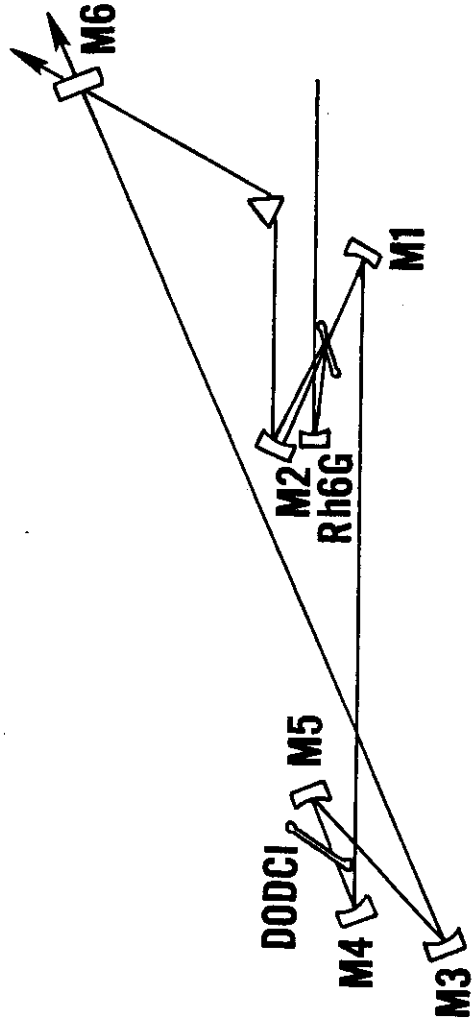
M6
M1
M2
Rh6G
M5
DODCI
M4
M3

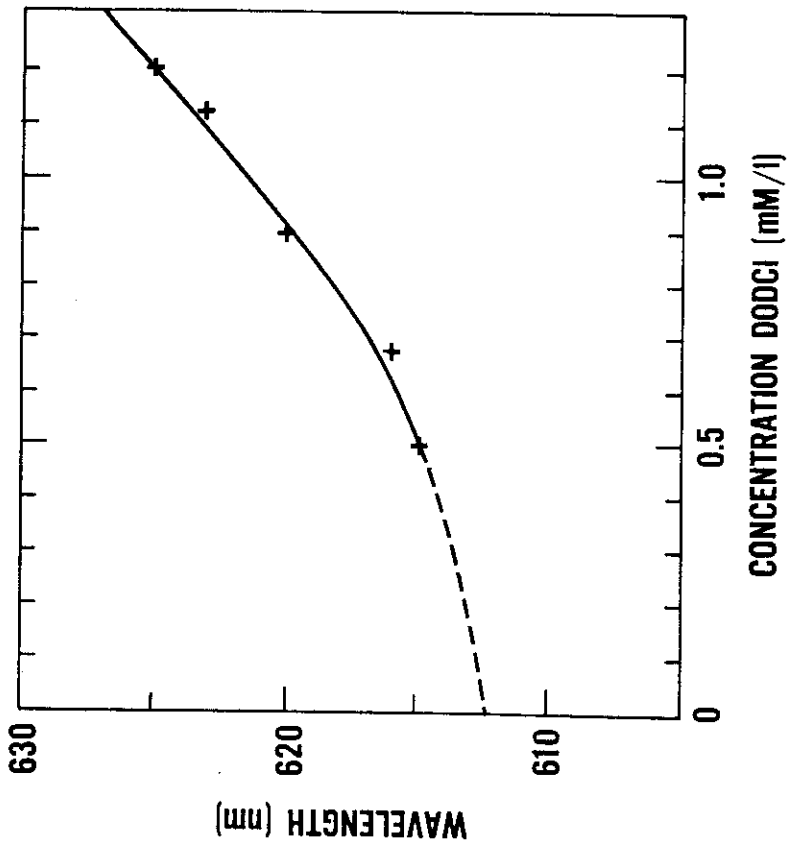
630
620
610
WAVELENGTH (nm)
0
0.5
1.0
CONCENTRATION DODCI (mM/l)

29

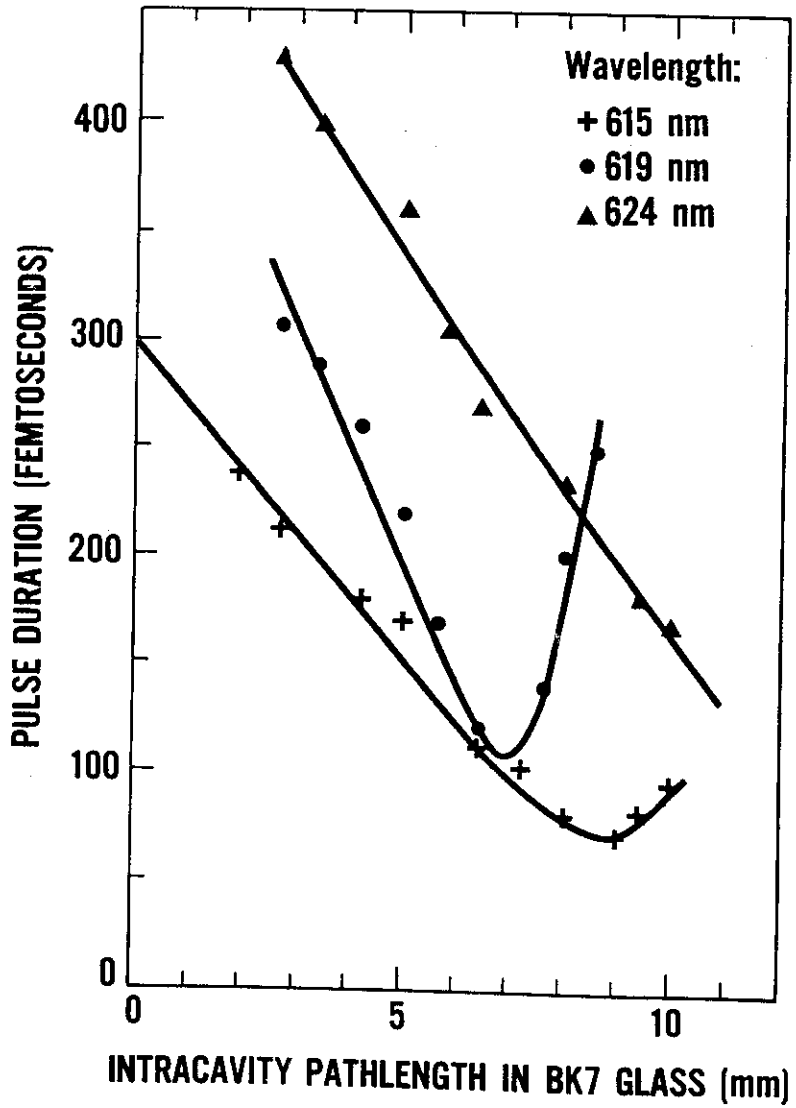
Wavelength:
+ 615 nm
• 619 nm
▲ 624 nm
400
300
200
100
0
PULSE DURATION (FEMTOSECONDS)
0
5
10
INTRACAVITY PATHLENGTH IN BK7 GLASS (mm)

30

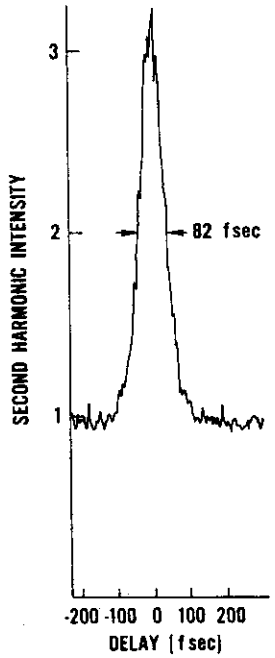
SECOND HARMONIC INTENSITY
3
2
1
82 fsec
-200 -100 0 100 200
DELAY (fsec)

Fig C

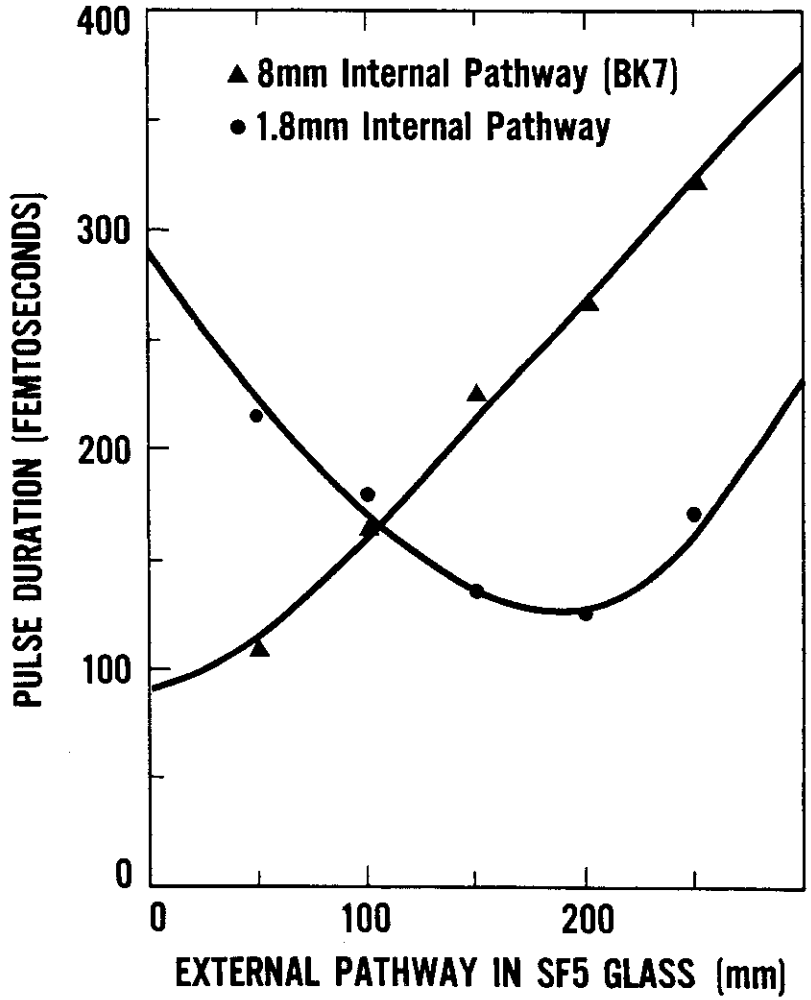
400
300
200
100
0
▲ 8mm Internal Pathway (BK7)
● 1.8mm Internal Pathway
PULSE DURATION (FEMTOSECONDS)
0
100
200
EXTERNAL PATHWAY IN SF5 GLASS (mm)

Fig 6

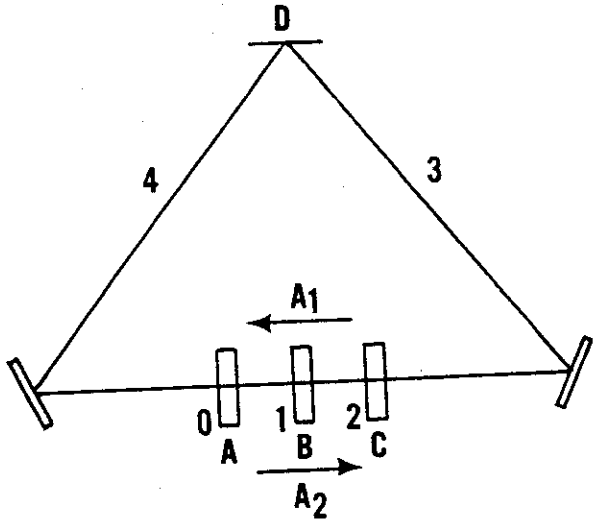

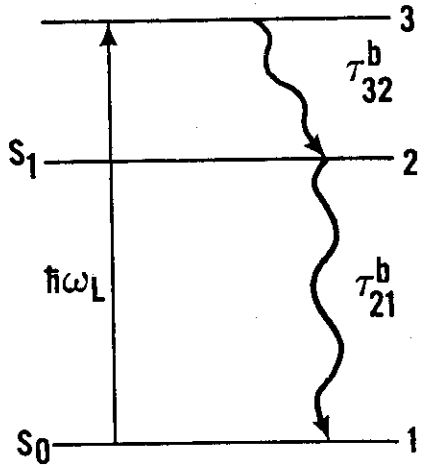

Fig 7

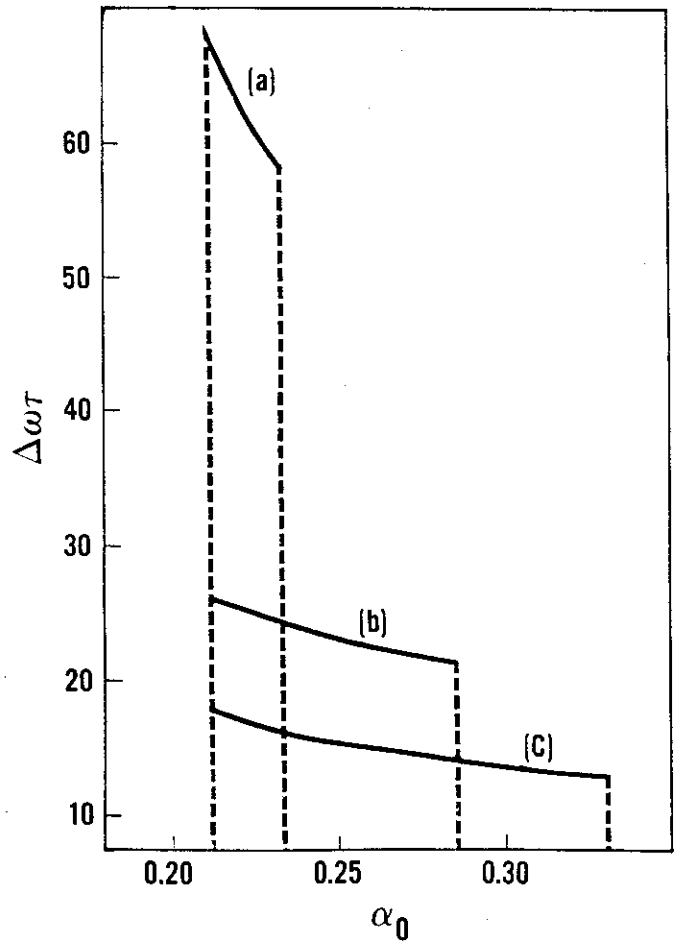
(a)
(b)
(C)
60
50
40
30
20
10
$\Delta\omega\tau$
0.20
0.25
0.30
α_0

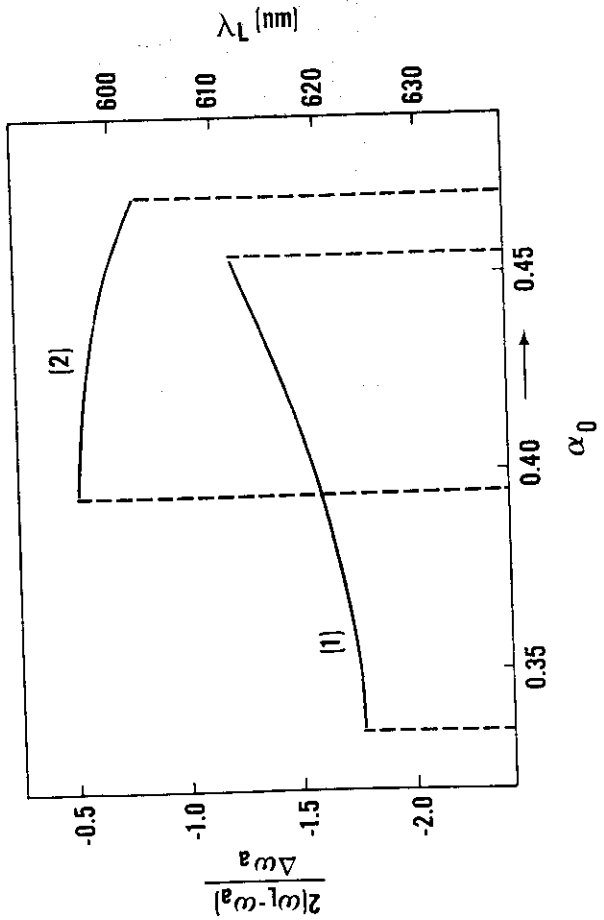
λ_L (nm)
600
610
620
630
(2)
(1)
0.45
0.40
0.35
α_0
-0.5
-1.0
-1.5
-2.0
$\frac{2(\omega_L-\omega_a)}{\Delta\omega_a}$

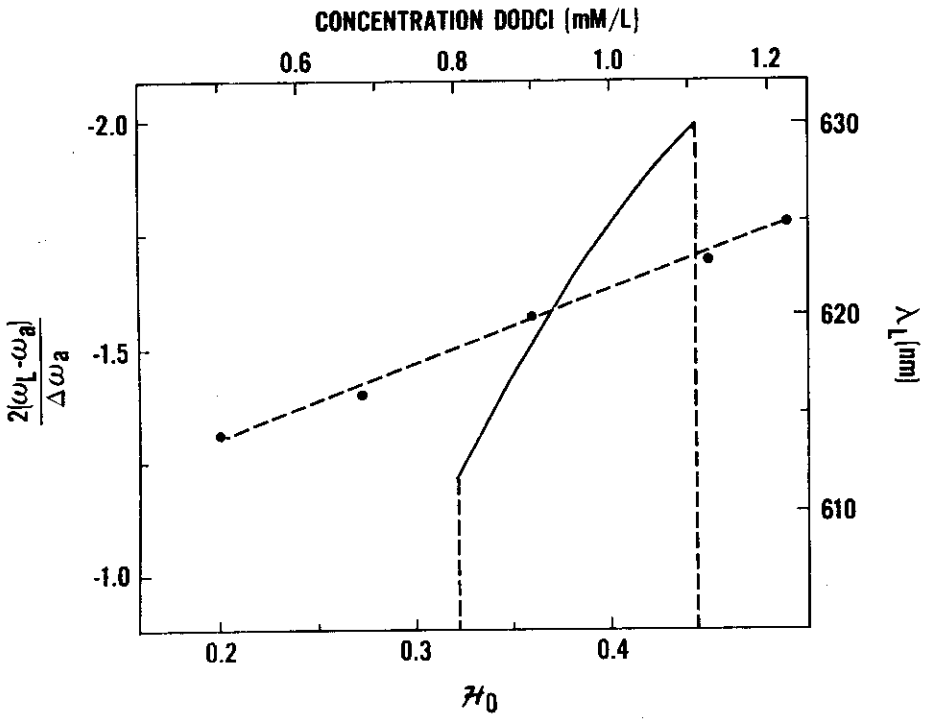
CONCENTRATION DODCl (mM/L)
0.6
0.8
1.0
1.2
-2.0
-1.5
-1.0
630
620
610
$\frac{2(\omega_L-\omega_a)}{\Delta\omega_a}$
λ_L (nm)
0.2
0.3
0.4
$\mathcal{H}_0$

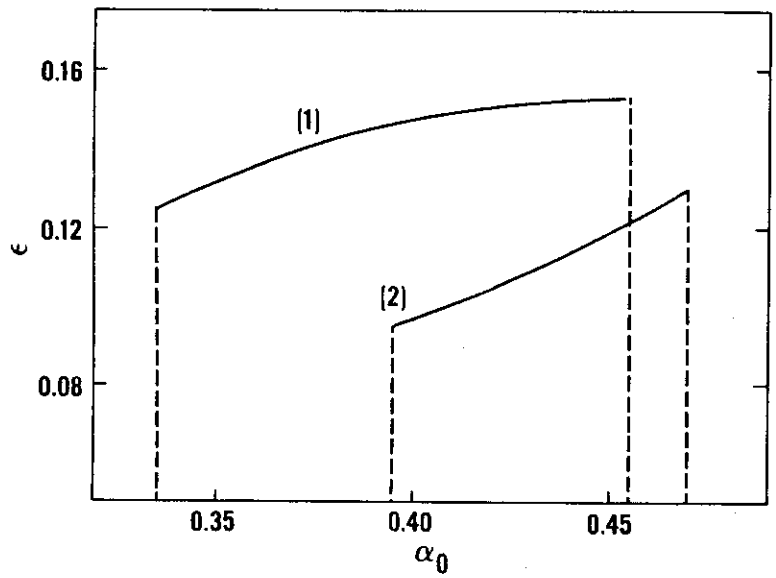
0.16
0.12
0.08
ϵ
(1)
(2)
0.35
0.40
0.45
α_0

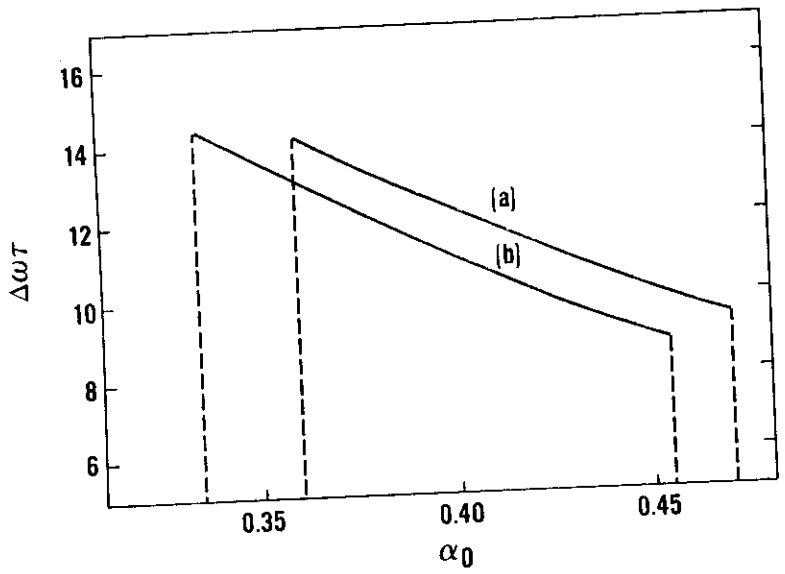
16
14
12
10
8
6
$\Delta\omega\tau$
(a)
(b)
0.35
0.40
0.45
α_0

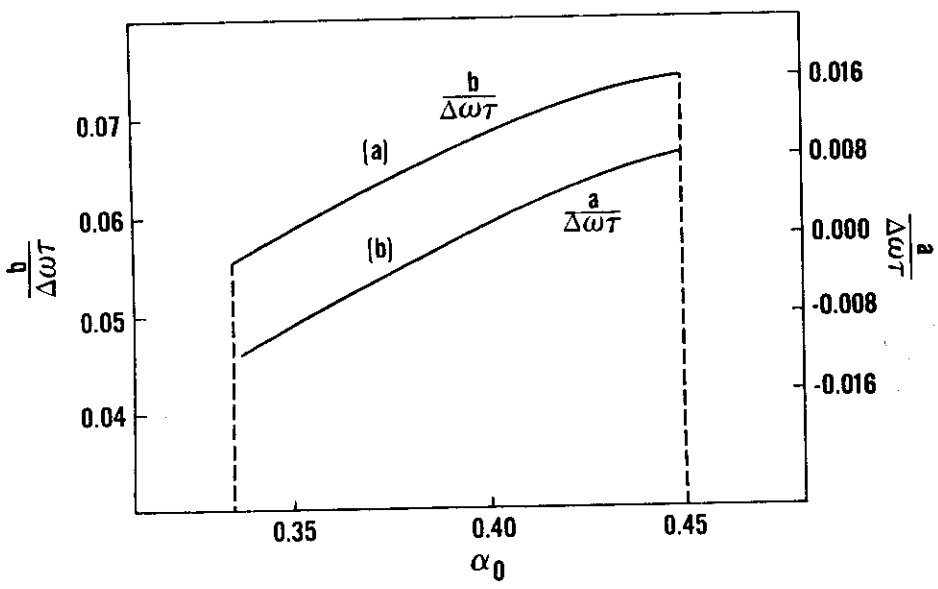
0.07
0.06
0.05
0.04
$\frac{b}{\Delta\omega\tau}$
$\frac{b}{\Delta\omega\tau}$
(a)
(b)
$\frac{a}{\Delta\omega\tau}$
0.016
0.008
0.000
-0.008
-0.016
$\frac{a}{\Delta\omega\tau}$
0.35
0.40
0.45
α_0